Accepted Manuscript

Electrochemistry of cyclic triimidazoles and their halo derivatives: A casebook for multiple equivalent centers and electrocatalysis

Mirko Magni, Elena Lucenti, Andrea Previtali, Patrizia Romana Mussini, Elena Cariati

PII: S0013-4686(19)31079-5

DOI: https://doi.org/10.1016/j.electacta.2019.05.146

Reference: EA 34287

To appear in: *Electrochimica Acta*

Received Date: 26 March 2019

Revised Date: 25 May 2019

Accepted Date: 28 May 2019

Please cite this article as: M. Magni, E. Lucenti, A. Previtali, P.R. Mussini, E. Cariati, Electrochemistry of cyclic triimidazoles and their halo derivatives: A casebook for multiple equivalent centers and electrocatalysis, *Electrochimica Acta* (2019), doi: https://doi.org/10.1016/j.electacta.2019.05.146.

Electrochemistry of Cyclic Triimidazoles and their Halo Derivatives: a Casebook for Multiple Equivalent Centers and Electrocatalysis

Mirko Magni [a,*], Elena Lucenti [b], Andrea Previtali [a], Patrizia Romana Mussini [a], Elena Cariati [a,b]

[a]*Department of Chemistry, Università degli Studi di Milano and INSTM RU, via Golgi 19, 20133 Milano, Italy*

[b]*Institute of Molecular Science and Technologies of CNR and INSTM RU, via Golgi 19, 20133 Milano, Italy*

Corresponding Author email: mirko.magni@unimi.it

ABSTRACT

A family of cyclic triazines, based on the triimidazo[1,2-*a*:1',2'-*c*:1",2"-*e*][1,3,5]triazine scaffold, has recently caught attention due to its variegated solid state photoluminescent properties (*e.g.*, crystallization induced emission, fluomechanochromis, dual fluorescence, room temperature ultralong phosphorescence), tuned by proper functionalization of the cyclic core. From an electrochemical point of view, this family of heteroaromatic cyclic triazines is unexplored. A cyclic voltammetry study is here performed aiming to clarify structure/electroactivity relationship. The peculiar molecular structure of this class of molecules offers a multi-approach case study, spanning from multiple equivalent redox site interactions in small hoops (due to ideally C_{3h} symmetry) to carbon-halogen bond reactivity in the presence of catalytic metal electrode surfaces (for –Br and –I derivatives). Results point to a poor heteroannular aromaticity along the rigid, planar cyclotrimer, with each equivalent redox site acting quite independently. An unusually higher electrocatalytic performance of gold with respect to silver electrode for the electrocleavage of carbon-halogen bonds (that decreases by increasing number of halo substituents) is tentatively explained in term of a specific interaction between gold and the nitrogen-rich planar cyclotrimer platform.

Keywords: cyclic triazines; multiple equivalent redox sites; electrocatalysis; carbon-halogen bond; dissociative electron transfer.

Declarations of interest: none

1. Introduction

Purely organic materials showing solid state room temperature phosphorescence (RTP) are receiving an ever growing interest due to their advantages with respect to the organometallic counterparts. In particular, their lower toxicity, cost and environmental load, together with more specific features such as long afterglow lifetimes, make them appealing in different fields spanning from anti-counterfeiting technologies, temperature monitoring, sensing and bio-imaging [1],[2],[3].

In organic solid RTP compounds the role of the crystal packing is that of suppressing molecular motions which work as non radiative deactivation channels for triplet excitons. In addition, densely packed structures can protect from oxygen quenching. However, more specific intermolecular interaction (*e.g.*, H aggregates) can be decisive in activating RTP [4].

We have recently reported on the intriguing photophysical behaviour of triimidazo[1,2-*a*:1',2'-*c*:1",2"-*e*][1,3,5]triazine, **TT**, its isomer (namely triimidazo[1,2-*a*:1,2-*c*:1,5-*e*][1,3,5]triazine, **iso-TT**) [5], and its mono-, di- and tri-bromo together with mono- and di-iodo derivatives (namely 3-bromotriimidazo[1,2-*a*:1',2'-*c*:1",2"-*e*][1,3,5]triazine, **1BrTT**; 3,7-dibromotriimidazo[1,2-*a*:1',2'-*c*:1",2"-*e*][1,3,5]triazine, **2BrTT;** 3,7,11-tribromotriimidazo[1,2-*a*:1',2'-*c*:1",2"-*e*][1,3,5]triazine, **3BrTT**; 3-iodotriimidazo[1,2-*a*:1',2'-*c*:1",2"-*e*][1,3,5]triazine, **1ITT**; 3,7-diiodotriimidazo[1,2-*a*:1',2'-*c*:1",2"-*e*][1,3,5]triazine, **2ITT**) (Figure 1) [6],[7],[8].

Both **TT** and **iso-TT** are better emitters in their crystalline state than in solution, a behaviour known as crystallization induced emission (CIE) [9],[10]. Moreover, **TT** displays mechanochromic emissive properties, together with room temperature ultralong phosphorescence (RTUP) at ambient

conditions (1s) associated with H-aggregation of the molecules in the crystalline structure [5]. The presence of one, two or three heavy atoms (Br, I) on the **TT** scaffold greatly modifies both the molecular and the aggregate photophysical behaviour. In fact, **1BrTT**, **2BrTT**, **3BrTT**, **1ITT** and **2ITT**, are characterized by an even richer and complex photoluminescence with emissions spanning from dual fluorescence, H aggregate RTUP and molecular phosphorescence [6],[7],[8].

(Figure 1)

Considering the attractive properties and potentialities of this triimidazotriazine family, a deeper knowledge of its electronic properties as well as their relationship with the molecular structure appears fundamental. In this regard, electrochemistry represents a powerful tool to get thermodynamic, kinetic and mechanistic information about the electron transfers involving electroactive molecules, and to estimate energy levels besides energy level differences (an intrinsic limitation of spectrophotometric technique) as well as to study possible interaction between redox sites.

The triimidazotriazine compounds (Figure 1) can be regarded from the electrochemical point of view as a very interesting and so far practically unexplored casebook study, on account of:

i) the high symmetry (ideally C_{3h}) of the cyclic triimidazole scaffold, in the perspective of studying multiple equivalent redox site interactions in small hoops;

ii) the systematicity of the available compounds, which allows an easy identification of structure vs electroactivity relationship;

iii) the presence of a series of halide members, whose electroactivity can be enhanced and modulated by the use of catalytic electrode surfaces.

In this context, the present work provides an exhaustive electrochemical study of the family of molecules reported in Figure 1. The halo-derivatives have been also investigated in view of possible

catalytic effect by specific metal surfaces (*i.e.*, silver and gold) toward the electroreductive cleavage of C–Halo (C–X) bond.

2. Experimental

2.1. Synthesis

All reagents and model molecules **Me_2-Im** and **Br-Im** were purchased from chemical suppliers and used without further purification unless otherwise stated.

TT, **iso-TT**, **1BrTT**, **2BrTT**, **3BrTT**, **1ITT**, **2ITT**, and **PyTT** were prepared according to literature procedures. In particular, **TT** and **iso-TT** were prepared by thermolysis of solid copper imidazolate $Cu(C_3H_3N_2)_2$ (Chart S1 in the Electronic Supporting Information)[11]. **1BrTT**, **2BrTT** [6] and **3BrTT** [7] were prepared by bromination of **TT** with respectively 1, 2 and 3.3 equivalents of N-Bromosuccinimide (NBS) at room temperature (Chart S2). **1ITT** and **2ITT** were prepared by iodination of **TT** with respectively 1 and 2 equivalents of *N*-Iodosuccinimide (NIS) and catalytic trifluoroacetic acid (TFA) in acetonitrile at room temperature (Chart S3) [8]. **PyTT** was prepared according to literature procedures [12] by Stille coupling between **1BrTT** and 2-(tributylstannyl)pyridine (Chart S4).

^{1}H and ^{13}C NMR spectra were recorded on a Bruker AVANCE-400 instrument (400 MHz). Chemical shifts are reported in parts per million (ppm) and are referenced to the residual solvent peak (MeOH, ^{1}H 3.31 ppm, ^{13}C 49.00 ppm). Mass spectra were recorded on a Thermo Fisher LCQ Fleet Ion Trap Mass Spectrometer equipped with UltiMate™ 3000 HPLC system.

2.1.1. Synthesis of 1-methyltriimidazo[1,2-*a*:1',2'-*c*:1'',2''-*e*][1,3,5]triazin-1-ium trifluoromethanesulfonate ($MeTT^+$)

(Chart 1)

In a 100mL one-necked flask with a magnetic stirrer, cyclic triimidazole **TT** (200 mg, 1.00 mmol) is dissolved in 30 mL of CH_2Cl_2 and added with methyl trifluoromethanesulfonate (0.45 mL, 3.97 mmol). The formation of a precipitate is observed after few minutes. The reaction is stirred at room temperature for 6 hours, filtered on a Buchner and the precipitate is washed thoroughly with CH_2Cl_2. Crystals of **MeTT**$^+$ are obtained by slow evaporation from MeOH (325 mg, yield 90%).

^{1}H NMR data (400 MHz, CD_3OD, 298 K, δ, ppm): 8.46 (d, 2.0 Hz, 1H), 8.42 (d, 2.4 Hz, 1H), 8.15 (d, 1.7 Hz, 1H), 7.97 (d, 2.4 Hz, 1H), 7.57 (d, 2.0 Hz, 1H), 7.52 (d, 1.7 Hz, 1H), 4.36 (s, 3H).

^{13}C NMR data (101 MHz, CD_3OD, 298 K, δ, ppm): 132.28 (*C*H), 131.34 (*C*H), 125.22 (*C*H), 114.56 (*C*H), 114.34 (*C*H), 113.23 (*C*H), 37.13 (*C*H_3).

MS (ESI-positive ion mode): *m/z* 213.1 $[M]^+$.

See Electronic Supporting Information (ESI) for NMR spectra (Figures S1,S2) and for HPLC-MS results (Figure S3).

2.2. Electrochemical measurements

Electrochemical characterization of cyclic triimidazole family was carried out in a three-electrode minicell filled with 3-4 cm^3 of solution containing ca. $7.5 \cdot 10^{-4}$ M of the sample dissolved in *N*,*N*-dimethylformamide (DMF) or acetonitrile with 0.1 M tetrabutylammonium hexafluorophosphate ($TBAPF_6$) as supporting electrolyte. Solution was well deaerated by bubbling N_2 into solution and by keeping a flux of gas just above the solution surface during all measures. A platinum wire was used as counterelectrode and an aqueous saturated calomel electrode (SCE) as reference one. To limit leakage of water and/or chlorides from SCE to the working medium, the reference electrode was inserted into a glass jacket, filled with the blank solution (solvent + $TBAPF_6$), ending with a porous septum which assures electric contact with the outside working solution. The recorded potentials were subsequently referred to the reference redox couple Fc^+|Fc (ferrocenium|ferrocene)

[13] added as external standard (*ca.* $1 \cdot 10^{-3}$ M) in a blank solution at the end of each daily measures ($E_{1/2}(Fc^{+}|Fc) \approx 0.50$ V and 0.39 V vs SCE in DMF and acetonitrile, respectively).

Three different working electrodes were employed during the characterization; glassy carbon disk electrode embedded into glass (GC, geometric area 0.031 cm^2, Metrohm) was taken as ideally inert (*i.e.*, non catalytic) substrate; teflon-embedded gold (Au, geometric area 0.031 cm^2, Amel) and silver (Ag, geometric area 0.071 cm^2, Amel) disk electrodes were selected to study the electrocatalytic behaviour of these metals toward carbon-halogen bond cleavage. Particular care was taken to the mechanical cleaning of the working electrode surface, employing synthetic diamond (for GC) or alumina powder (for Ag and Au) suspended in deionized water on a piece of polishing cloth (Struers®).

Cyclic voltammetry was used for the electrochemical characterization by employing an Autolab PGSTAT302N potentiostat/galvanostat managed by a PC with GPES software. An instrumental compensation of the resistance (*i.e.*, positive feedback technique) was carefully performed in order to minimize the ohmic drop between the working and reference electrode.

3. Results ad Discussion

3.1. Non-halogenated triimidazoles

The study was performed almost entirely in DMF, according to its good solvent capability for all the studied compounds. The forefather triimidazo[1,2-*a*:1′,2′-*c*:1″,2″-*e*][1,3,5]-triazine, **TT**, (Figure 1) exhibited a poor electrochemical reactivity on glassy carbon, GC, electrode in DMF with 0.1 M $TBAPF_6$ (Figure 2). Notwithstanding the wide available potential window offered by the working medium (ca. 4.6 V), reduction and oxidation peaks of **TT** are only partially resolved at background discharge limits. The recalcitrant redox activity, especially toward reduction, is attributable to the weakly π-excessive nature of each heteroaromatic five-member ring [14]. Oxidation is probably hampered mainly by 1,2-annelation that precludes prototropic annular tautomerism between the two nitrogens of each imidazole [15].

(Figure 2)

Oxidation of **TT** can be studied more easily in acetonitrile. Within the wider oxidation potential window offered by this solvent, the molecule shows a peak at 1.38 V vs $Fc^+|Fc$ (at 0.2 V s^{-1} potential sweep, see Figure S4) associated to a chemically irreversible process (up to 10 V s^{-1}); the peak moves toward more positive potentials by increasing the potential scan rate υ (ca. 0.03 V/dec). To better understand structure-reactivity relationship of the **TT** scaffold, other analogues were considered, starting from 1,2-dimethyl-1*H*-imidazole, **Me_2-Im**, (Figure 1) taken as model for the 1,3-diazole constituting unit. According to the inductive donor nature of the methyl groups reduction is more difficult while oxidation is easier than for **TT,** resulting in an anodic peak, $E_{p,a}$, at 1.00 V vs $Fc^+|Fc$ at 0.2 V s^{-1} (Figure 2) without a cathodic counterpart up to 10 V s^{-1} potential sweep. The peak potential shift ($\partial E_{p,a}/\partial \log\upsilon$) of 0.04 V toward more positive potentials by increasing sweep rate, υ, points to an electrochemically quasi-reversible electron transfer followed by a fast chemical reaction step, in very good quantitative agreement with previously reported data for related 1,2-dimethyl-benzimidazole [16]. The ca. 100 mV negative shift for the oxidation of **Me_2-Im** with respect to the latter could be due to the more π-deficient nature of the benzannulated compound According to the few reported papers [15], this process is attributable to a monoelectronic electron transfer, ET, which converts the neutral reagent into the corresponding radical cation mainly centred on the pyridine-like nitrogen. Imidazole N,N electropolymerization, following a $1e^-$-$2H^+$ mechanism [15], is prevented by alkylation of the pyrrole-like nitrogen. A further proof of the monoelectronic nature of the voltammetric signal of **Me_2-Im** is provided by comparing the limiting current of the steady state curves obtained by convolution of the experimental peak-shape CV patterns of **Me_2-Im** and ferrocene, the last being selected as reference compound (Figure S4, right).

A useful clue to evaluate the interaction among each equivalent imidazole unit in **TT** is the comparison of the peak current (and/or of the related exchange charge) with respect to the model **Me_2-Im**. While the anodic peak of **TT** in DMF is too positive to enable a reliable quantitative estimation, acetonitrile makes it possible. Comparison of the peak currents and, even better, of the pseudo-limiting currents of the convoluted voltammetric curves clearly shows that oxidation of **TT** involves more than one electron (Figure S4), being the current of **TT** around two-times higher than that of **Me_2-Im** (keeping constant their concentration). Taking into consideration the lower diffusion coefficient (which reduces both peak and limiting current) expected for the triimidazole according to the significant differences in steric hindrance and molecular weight with respect to **Me_2-Im**, an electron transfer involving all the three equivalent sites of **TT** seems to be plausible.

The absence of any degeneration loss of the voltammetric peak is another important diagnostic tool to sustain the independency of the equivalent imidazole rings in **TT**, since any electronic communication of the units should invariably result into a splitting of the oxidation process in more than one peak, the first one being negatively shifted (as a result of the increased conjugation) with respect to the referring **Me_2-Im**. Nonetheless, considering the last observation and also that each methyl group should contribute an inductive-based negative potential shift of ca. 0.05 V, the ca. 0.35 V positive shift for the oxidation of **TT** with respect to **Me_2-Im** in acetonitrile points to each equivalent imidazole ring being a (nearly) independent redox site; the resulting extra positive shift of **TT** also accounts for the electron-withdrawing inductive effect of imidazole rings as substituents. This conclusion could be in contrast with the proposed thesis that a moderate heteroannular aromaticity could exist along the rigid, planar cyclotrimer constituted by a 18 π-electron system, as supported by UV absorption and NMR data [17]. The conflict can be attenuated considering that, actually, the cited work provided no conclusive proof and that the relative permittivity (36.7 and 37.5, for DMF and acetonitrile, respectively [18]) of the solvents used in the current work can provide a quite efficient charge shielding effect that minimizes interactions between the redox sites. A further inside discussion is postponed to the study of multi halo-**TT**s (section 3.2.1.2).

Introduction of a heteroaromatic substituent on the imidazole ring brings to deep modifications in the electrochemical reactivity of the resulting **pyTT** (Figure 1). The electrochemical gap is significantly reduced probably due to the mesomeric effect of pyridine that, being expected to form a relatively small dihedral angle with the linked imidazole, offers a suitable conformation to increase the effective π-conjugation that synergistically favours both oxidation and reduction. A similar effect induced by a variation in conjugation was already reported for bibenzimidazoles [16]. Major modifications concern the reduction, which could involve both cyclotriazine and pyridine, with the appearance of two distinguishable peaks corresponding to fast ETs ($\partial E_{p,c}/\partial \log \upsilon \approx 0.03$ V). The first one can be an electrochemical-chemical coupled process (EC) generating a radical anion with subsequent chemical follow-up with relatively low rate constant, accounted for by observation of an increasing return peak with increasing scan rate (see Electronic Supporting Information, Figure S5). This finding points to a follow-up reaction slow enough to only negligibly compete with a second electron transfer; the latter generates a dianion, which, being a stronger base, is probably protonated by trace water molecules to form a monoanion. This second peak shows a small anodic partner at around –0.7 V *vs* $Fc^+|Fc$, attributable to monoanion oxidation, only visible at scan rates slower than 1–2 Vs^{-1} (Figure S5). Considering the easier reducibility of pristine pyridine with respect to **TT** core (E_p = –3.10 V *vs* $Fc^+|Fc$ [19] and around –3.25 V *vs* $Fc^+|Fc$, respectively) it is plausible that the first ET is localized on the heteroaromatic substituent, whose potential is positively shifted due to the partial conjugation with cyclotriazine core.

A CV pattern characterized by two subsequent reductions (Figure 2) was recorded also for the salt obtained by methylation of one nitrogen atom of the triimidazole, **MeTT**$^+$ (Figure 1). In this case the chemical modification, aimed at understanding the effect of the charge on the molecule (neutral in **TT**), results in the most reducible species in the studied series accordingly to its electron deficient nature. On the other hand oxidation, which was superimposed to the background for

neutral **TT**, is no longer accessible, being shifted toward a more extreme potential. Actually, similarities with **pyTT** pattern disappear when the two reduction peaks are analyzed in more details, revealing an ECE type mechanism. In fact, the ratio of the current densities after normalization for the sweep rate ($j/cv^{1/2}$) for the second peak with respect to the first one increases upon slowing down the scan rate potential (Figure S6) and a cross-point between currents recorded during forward and backward scan appears. Similarly to an analogue study on 1,2,3-trimethyl-benzimidazolium salt [16], the first quasi-reversible electron transfer at –2.14 V vs $Fc^+|Fc$, centred on the electron-poor alkylated nitrogen, is followed by a fast chemical follow up reaction (*i.e.*, the ET is irreversible up to the highest applied scan rate of 2 V s^{-1}, Figure S6). The last converts the electrogenerated neutral radical into a new species that is reduced at more negative potential, –2.67 V vs $Fc^+|Fc$, in a process that is partially chemically reversible at faster potential scan rates. The detailed nature of these reactions was no further investigated.

Isomer **iso-TT** (Figure 1), resulting from one 1,5-annelation, is more redox active than the more symmetric 1,2-annelation product **TT** (Figure 2), in agreement with its lower stability (an hence more reactivity) predicted by DFT calculation [20]. Oxidation is probably localized on the isomerised imidazole according to the high regioselectivity shown by the N-alkylation reaction [19],[20]; the 50-60 mV shift in the negative direction with respect to **TT** is again explained by the greater electron-richness of this imidazole. On the other hand the reduction, occurring at almost the same potential than in the major isomer, is centred on the almost equivalent 1,2-annelated moieties.

3.2. Halogenated triimidazoles

3.2.1. Glassy carbon electrode: intrinsic features

Carbon–halogen bond (C–X) has been object of great attention because its electro-cleavage has represented for electrochemists a model case for the investigation of dissociative electron transfer (DET) processes [21]. As pointed out by Saveant and co-workers [21],[22],[23],[24] the process can

occur through two limit mechanisms, stepwise and concerted. In the first scenario electron transfer produces a transient radical anion $RX^{\bullet -}$ which then undergoes rupture of the carbon-halogen bond (eqs. 1 and 2, respectively).

$RX + e^- \rightarrow RX^{\bullet -}$ (eq. 1)

$RX^{\bullet -} \rightarrow R^{\bullet} + X^-$ (eq. 2)

In contrast, in the concerted mechanism electron transfer and bond breaking are concurrent, with the direct formation of $R^{\bullet}$ and X^- (eq. 3).

$RX + e^- \rightarrow R^{\bullet} + X^-$ (eq. 3)

Generally speaking, DET follows the stepwise pathway with aromatic halides (due to the presence of low lying π^* orbitals suitable to transitorily stabilize the incoming electron) and the concerted one with alkyl derivatives (for which the injection of an electron leads to a purely dissociative state). Nevertheless several anomalies to this rule or transition between the two mechanisms have already been reported [23], [24], [25], [26], [27]. In addition, the solvent (and its proticity) resulted as a key parameter in determining the preferred pathways between the two [28],[29],[30].

In this context halogen derivatives of **TT** represent an interesting novel case study useful to enrich the already available ensemble of compounds that despite counting plenty of examples of carbon-based molecules, spreading from aliphatic (*e.g.*, alkyl, benzyl, nitrile) to aromatic halogens, is quite poor in term of the heteroaromatic, in particular N-heteroaromatic, analogues.

Before considering the halo-**TT** derivatives, it is instructive to analyze the behaviour of their model molecule, namely 5-bromo-1,2-dimethyl-1*H*-imidazole, **Br-Im**, (that is the bromo derivative of **Me_2-Im**, Figure 1). Contrary to **Me_2-Im**, that does not show any reduction in the available potential window, the cyclic voltammetry pattern of **Br-Im** is characterized by a reduction peak just before the background discharge (Figure 3).

(Figure 3)

The peak potential, around –3.26 V vs $Fc^+|Fc$ at 0.2 Vs^{-1}, linearly moves toward more negative values with increasing potential scan rate ($\partial E_{p,c}/\partial \log \upsilon$=0.09 V) suggesting a kinetically controlled ET chemically irreversible in nature, due to absence of any anodic part (see Figure S7). The diffusive current of the reduction peak is compatible with the exchange of two electrons per molecule taking the oxidation peak of the analogue **Me_2-Im** as reference for a monoelectronic ET, as previously stated. All these features suggest that the investigated process directly involves the halogen atom resulting in hydrodebromination of the starting molecule. Firstly, the aforementioned DET results in the electrocleavage of C–Br bond with the formation of bromide ions, Br^-, and radical $Im^{\bullet}$, the last being further reduced to anion Im^- through a second monoelectronic ET at the same electrode potential of the DET (*i.e.*, reduction potential for $Im^{\bullet}|Im^-$ couple is more positive than $E_{p,Br\text{-}Im|Im^{\bullet}}$). Observation of possible subsequent reduction steps for the anion (or of its protonated form, ImH, resulting from self-protonation or abstraction of H^+ from solvent or residual water molecules) is precluded by the background signal. Discriminating between the two limiting mechanisms of DET further increases the knowledge for this new class of halo-imidazole. According to literature [19],[21],[26],[30],[31], as the investigated process is irreversible and under diffusion control, the kinetic parameter κ can be calculated according to either peak width (eq. 4) or peak potential variation with sweep rate (eq. 5).

$$\kappa = -\frac{1.857RT}{F(E_p - E_{p/2})} \quad \text{(eq. 4)}$$

$$\kappa = -\frac{1.51RT}{F(\partial E_p / \partial \log \upsilon)} \quad \text{(eq. 5)}$$

When 0.5<κ<1 the DET proceeds through a stepwise mechanism, with chemical barrier (eq. 2) being the rate determining step. If 0.35<κ<0.5 the process is still stepwise but the electrochemical barrier (eq. 1) prevails on the chemical one. Finally if κ<0.35 the DET follows a concerted reaction pathway (eq. 3). Actually the kinetic parameter κ corresponds to the transfer coefficient (also known as “symmetry factor”), α, when κ<0.5.

The parameter κ (from now on called α, being <0.5 for all samples, see Table 1) for **Br-Im** on GC electrode is 0.32, both employing eqs. 4 and 5.

(Table 1)

This finding points to a concerted DET, with electron transfer and bond cleavage concurrently occurring. This is an interesting result because, even if some exceptions already exist (as above reported), aryl halides commonly undergo a stepwise DET with the transitional formation of a radical anion stabilized by the presence of a low energy π^* orbital. To the best of our knowledge, 3-halo-pyridines are one of the very few examples of N-heteroaromatic halides for which DET studies have been reported [19]. In particular, 3-bromo-pyridine (selected as the most similar to our model **Br-Im**) follows a stepwise mechanism, with an average κ value of 0.59 [19]. Being the last parameter >0.5 it is reasonable to consider that the rate determining step of the process is the bond breakdown. Considering a comparable bond dissociation energy, BDE, for the C–Br bond in the two N-heteroaromatic halides, it is plausible that **Br-Im** is forced to follow the concerted pathway simply because the absence of a π^* orbital (LUMO) sufficiently low in energy precludes any thermodynamically favourable formation of the radical anion intermediate. As a result, electron density is mainly localized on the C–Br bond [32]. A similar comment applies for the comparison with bromo-thiophenes [31]; the higher aromaticity of the five-member S-heteroaromatic ring with respect to the N,N-analogue could explain the stepwise mechanism of the DET for the series of variably substituted bromo-thiophenes. In this case the values of the transfer coefficients ($0.35<\alpha<0.50$) points to the energy barrier for the electron transfer step be more important than that for the chemical one.

3.2.1.1. Mono-halogenated TT

Functionalization of the cyclotrimer scaffold with a –Br (**1BrTT**) and –I (**1ITT**) substituent (Figure 1) determines a ~0.3 V and ~0.75 V shift of the reduction peak toward more positive potentials with respect to the benchmark **TT**, respectively (Table 1). This shift cannot be merely attributed to the depletion of the electron density on the **TT** core as a consequence of the inductive electron withdrawing effect of the halogens. In fact, for sake of comparison, introduction of –Br and –I on one of the cyclopentadienyl rings of ferrocene (chosen as reference for an outer sphere ET, centred on the metal core) only results into a 150 mV positive shift of the standard potential for the oxidation, with a negligible difference between the two halogens [33]. So, analogously to the case of model compound **Br-Im**, the electron transfer should involve a completely different molecular site with respect to that of the pristine **TT**: the carbon–halogen bond, that is subjected to a dissociative electron transfer. Both halo-derivatives exhibit one diffusive, totally irreversible bielectronic peak associated to the hydrodealogenation of the reagents. The slightly lower peak current of **1ITT** with respect to **1BrTT** is plausibly attributable to its lower diffusion coefficient on account of the bulkier iodine atom. On GC electrode, **1BrTT** and **1ITT** showed identical symmetry factors (α=0.32, Table 1), equalling that of the bromo-model too. As a consequence DET still occurs with a concerted mechanism independently of the presence of three 1,2-annelated imidazole rings (with respect to the reference compound, **Br-Im**). This finding can further reinforce the thesis, previously discussed in section 3.1, that each imidazole unit in the cyclotrimer acts as an almost independent redox site, minimizing (or avoiding) the heteroannular aromaticity that should result in a more stable LUMO and, hence, in the promotion of the competing stepwise pathway for the DET.

The 450 mV positive shift of E_p going from **1BrTT** to **1ITT** (Table 1 and Figure 3) is well known [19], being related to the C–X bond dissociation energy ($BDE_{C–Br}$>$BDE_{C–I}$) that affects both thermodynamics [21] and kinetics of concerted DET processes [22]. In particular, BDE of 2.97 and 2.33 eV can be estimated for the –Br and –I derivative from eq. 6 [24]

$$BDE = \frac{2}{3}\left(E^0_{X\bullet|X-} - E_p\right) + 0.3 \quad \text{(eq. 6)}$$

where E_p is the reduction peak potential at 0.2 Vs^{-1} (Table 1), $E^0_{Br•|Br-}$ = 1.48 V *vs* SCE and $E^0_{I•|I-}$ = 0.99 V *vs* SCE [26], and converting the potential scale reference from SCE to $Fc^+|Fc$ by using the experimental average value $E_{1/2,Fc+|Fc}$ = 0.49 V vs SCE.

3.2.1.2. Multi-halogenated TT

A given analyte can undergo multiple subsequent electron transfers localized on different sites of its molecular structure; these sites can be equivalent or not. Since many years, communication between redox sites (especially if they are equivalent) has represented an attractive research field for many electrochemists [34], with interesting applications even in bio(electro)chemistry [34],[35].

Modification of the **TT** scaffold with two (**2BrTT** and **2ITT**) or even three (**3BrTT**) halogen atoms (Figure 1) gives raise to some derivatives which represent a valuable model systematic series to study at the same time i) the interaction between equivalent redox sites and ii) DET on multi-halogenated heteroaromatic compounds, of which only a limited case number is so far available. Actually, in the cited compounds the C_{3h} symmetry of the **TT** core and the regioselectivity of halogenation (conducted on the C5 carbon atom of each imidazole) assure the equivalence of the C–X bonds.

The low solubility of some of the multi-halogenated compounds and the quite negative reduction potential (especially for bromo derivates) forced measurements to be carried out in DMF, on account of its very recalcitrant reduction discharge, notwithstanding its high relative permittivity [18], with related significant charge shielding ability, resulting in less evident multiple redox site interactions respect to more apolar solvents.

The electrocleavage of C–X bond is invariably characterized by a unique peak whose potential (Table 1 and Figure 3) is only slightly influenced by the number of halogens. From the mechanistic point of view DET is not modified, except for a small decrease of α by increasing the number of halogens (from 0.32 to 0.27, going from **1BrTT** to **3BrTT**, Table 1). Invariance of both multiplicity and potential of the peaks is in clear contrast with what previously reported for multi-

bromothiophenes for which the number of the reduction peaks (separated by ca. 0.4 V) increases with the number of –Br units and a shift of the first peaks towards positive potentials was observed, according to the increasing cumulative electron withdrawing effect of the halogens [31]. These two findings suggested that in thiophenes the equivalent redox sites (*i.e.*, C–Br bonds) are interacting; in particular, wider the distance between two subsequent peaks stronger the interaction between the equivalent sites [36]. In comparison, the present results for multi-halogenated **TTs** point, again, to an hampered communication between the imidazoles along the cyclic triimidazole planar structure. Actually some conjugation, albeit weak, through the 1,2-interannular bonds cannot be completely excluded, considering the charge shielding effect of the solvent and the following two experimental findings. The first one concerns the linear increase of peak current with the number of halogen substituents, even if the slope is significantly less steep than that expected for ideally interacting sites, even considering the expected progressive decrease in the diffusion coefficient (see Figure S8). The second proof is that at low scan rate (*i.e.*, 0.05 V s^{-1}) a shoulder at more positive potentials seems to appear for **2BrTT** and **3BrTT**, clearer if seen in differential mode (Figure S9). The peaks in differential mode (*i.e.*, the flex points in normal CV mode) are progressively shifted toward positive potentials by increasing –Br atoms due to the increased total inductive effect of substituents. On the other hand, such partial splitting was not recorded for **2ITT**.

3.2.2. Gold and silver electrodes: electrocatalytic DET

The aforementioned results provide a picture of the intrinsic electrochemical behavior of halo-triimidazotriazianes, considering the glassy carbon electrode as an inert surface (*i.e.*, a source of electrons transferred to the acceptor molecules in solution). However different metal surfaces, including silver, gold, copper and palladium demonstrated a particular affinity for halo-derivatives resulting in a catalytic effect toward DET processes not only in traditional organic solvents (aprotic and protic) [30] but also in room temperature ionic liquids [37]. On catalytic surfaces, and in particular on Ag, the mechanism proposed for outer sphere donors (*e.g.*, inert GC electrode) that

involves a “two-centre intermediate” R···X, is modified accounting for a “three-centre intermediate” R···X···M possibly through formation of more favourable activated complex and/or interaction of the metal electrode (M) with halogenated reactant and their reduction products and intermediates [32],[38]. As a result a positive shift (even up to ca. 1 V) of the DET peak can be observed with respect to the inert glassy carbon electrode. This “catalytic effect” can be quantified in term of the difference of the peak potential recorded on the catalytic and inert electrode, $E_{p,X}$–$E_{p,GC}$, with X stands for the catalytic electrode.

Behaviour of halo-**TTs** on gold (Au) and silver (Ag) electrodes are shown in Figure 4. Reduction peaks of all compounds are shifted toward more positive potential than the corresponding ones on inert GC substrate, with iodo derivatives being always more easily reduced according to the lower BDE of C–I. Mechanism of DET is in this case not affected by the electrode surface, unlike the possible stepwise-to-concerted switch reported for some bromo-aryls going from non-catalytic to catalytic (Ag) electrode [32]. Actually all available α values (depending on the peak features), being around 0.30 (Table 1), point out again to a concerted pathway with concomitant electron transfer and C–X bond cleavage even on Au and Ag electrode.

(Figure 4)

Very interestingly, the catalytic activity of Au electrode is invariably higher than that of Ag (Table 1) contrary to what commonly reported for halo-compounds. In fact, even if Au has the highest affinity for halide anions, according to both theoretical predictions [39] and experimental confirmations [40], its potential of zero charge (PZC) is so positive that in the potential range typical for RX the metal surface bears a large negative charge that decreases the affinity of Au for X^- due to strong coulombic repulsive forces. The more negative PZC of Ag implies significantly lower electrostatic repulsion resulting in a better catalytic effect for RX reduction.

In the specific case of halo-**TTs,** peak potentials for the bromo series (Table 1) are too much negative to allow adsorption of electrogenerated Br^- on Ag (adsorption threshold is –1.33 V vs SCE [41], corresponding to –1.82 V vs $Fc^+|Fc$ in our experimental conditions) and, even more, on Au electrode. This feature precludes any significant thermodynamic contributions from specific adsorption of Br^- products to the electrocatalytic reductive DET process. As a result the catalytic effect arises from a purely kinetic contribution, with metal surface reducing the energy barrier of the process for example by forming a favourable activated complex or by directly interacting with RX.

On the other hand, a thermodynamic contribution to the electrocatalysis of **1ITT** and **2ITT** should be also taken into consideration at least on Ag electrode because adsorption of I^- is relevant at potentials up to about –1.50 V *vs* SCE [41] (–1.99 V *vs* $Fc^+|Fc$), as experimentally confirmed by i) the sharp morphology of the main peak at about –1.85 V vs $Fc^+|Fc$ (Figure 4), which could be attributed to a hybrid diffusive-adsorptive ET process, and ii) the small adsorption pre-peak at about –1.45 V vs $Fc^+|Fc$ whose current linearly increases with the scan rate potential. This additional contribution can also account for the better catalytic effect of Ag toward iodo-TTs with respect to Br-TTs.

Nevertheless the lower catalytic effect of Ag with respect to Au (considering the main peak) even with iodoTTs suggests that this energetic contribution is minor with respect to the kinetic one. In conclusion the intrinsic electronic properties of Au seem to make this metal more effective than Ag in the interaction with triimidazotriazines. A tentative description of the molecule-surface interaction accounting for this kinetic catalysis can derived by the peculiar features of the **TT** scaffold: six nitrogen atoms acting as temporary “anchor sites” for the planar and rigid cyclotrimer. In this view N-atoms mimic the well documented adsorption of DNA strands on Hg electrode through nitrogenous bases [42]. In order to maximize the energy of the molecule-metal interaction (*i.e.,* the number of active anchors) the **TT** moiety should approach the electrode surface with a parallel orientation. The decrease in catalytic activity of both metal surfaces by increasing the number of halo substituents on **TT** core (within the **Br-TT** series it spans in the range 0.63-0.4 V on

Au and 0.50-0.41 V on Ag, and within **I-TT** one 0.94-0.88 V on Au and 0.73-0.68 on Ag; Table 1) can be well rationalized by the aforementioned thesis. In fact, the bulky halogen atoms, acting as spacer between the flat cyclotrimer (and hence its anchor nitrogens) and the surface of the metal, progressively hamper the interactions responsible for the lowering of the energy barrier for DET.

Reduction peak of **Br-TTs** on both Au and Ag electrode showed a non-canonical shape with respect to that on inert GC electrode. In particular pattern of the current during backward scan crosses that of the forward one at a potential few hundreds millivolt more positive than the peak potential. This current loop is typically observed when a soluble product of the EC reaction is more easily reducible than starting material or when the electrode surface is "activated" by an electrodeposited product [21].

4. Conclusions

The electrochemical activity of triimidazo[1,2-*a*:1′,2′-*c*:1″,2″-*e*][1,3,5]-triazine, **TT**, and related derivatives has been extensively investigated on different electrode surfaces.

First oxidation and first reduction of the **TT** system as such both require extreme potentials; oxidation is slightly promoted by isomerization of one imidazole (**iso-TT**), on account of the more electron-rich nature of the 1,5-annelated ring. Examples have also been provided of **TT** reactivity enhancement by inductive or conjugative effects of suitable substituents, with alkylation of a pyridine-like nitrogen (**MeTT**$^{+}$) and introduction of a heteroaromatic substituent (**pyTT**) both promoting reduction.

Despite the rigid, planar structure of the cyclotrimer platform, poor interaction between equivalent redox sites (each imidazole unit in **TT** and each C–halo bond in multi-halogenated compounds) has been observed. Unfortunately this does not represent a definitive proof to solve the open question related to the heteroannular aromaticity in **TT** scaffold [17], mainly because of the high relative permittivity of the solvent that could shield site interactions.

Bromo (**1BrTT**, **2BrTT**, **3BrTT**) and iodo (**1ITT**, **2ITT**) derivatives of cyclic triimidazole are subjected to reductive electro-cleavage of the C–X bond through a DET concerted mechanism, notwithstanding the aromatic nature of the imidazole unit, which by analogy with former aromatic cases was expected to favour a stepwise pathway. DET is significantly catalyzed by silver and gold electrode surfaces that reduce the cathodic potential to be supplied by up to 0.9 V. Even more interestingly, gold has revealed to be the best electrocatalyst, overcoming silver that commonly exhibits better performance in carbon-halogen electrocatalytic bond cleavage due to its more negative PZC and therefore lower negative charge density at the working potentials. A tentative explanation for this inversion has been proposed, relying on the presence of six nitrogen atoms close each others in a planar, rigid cyclotrimer.

A new case with very attractive peculiarities is thus added to the palette of organic halide families so far investigated concerning the fundamental process of electrocatalytic carbon-halide bond cleavage. In particular, with respect to the formerly investigated halo-thiophene case, it is confirmed and even better highlighted (by the neat inversion between Au and Ag) the essential role of heteroatoms in influencing the surface catalytic activity, by acting as "adsorption auxiliaries" possibly counteracting charge repulsion effects in the working potential range.

References

[1] M. Baroncini, G. Bergamini, P. Ceroni, Rigidification or interaction-induced phosphorescence of organic molecules, *Chem. Commun.* 53 (2017) 2081.

[2] S. Hirata, Recent Advances in Materials with Room-Temperature Phosphorescence: Photophysics for Triplet Exciton Stabilization, *Adv. Opt. Mater.* 5 (2017) 1700116.

[3] J. Mei, N. L. C. Leung, R. T. K. Kwok, J. W. Y. Lam, B. Z. Tang, Aggregation-Induced Emission: Together We Shine, United We Soar!, *Chem. Rev.* 115 (2015) 11718.

[4] A. Forni, E. Lucenti, C. Botta, E. Cariati, Metal free room temperature phosphorescence from molecular self-interactions in the solid state, *J. Mater. Chem. C* 6 (2018) 4603.

[5] E. Lucenti, A. Forni, C. Botta, L. Carlucci, C. Giannini, D. Marinotto, A. Previtali, S. Righetto, E. Cariati, H-Aggregates Granting Crystallization-Induced Emissive Behavior and Ultralong Phosphorescence from a Pure Organic Molecule, *J. Phys. Chem. Lett.* 8 (2017) 1894.

[6] E. Lucenti, A. Forni, C. Botta, L. Carlucci, C. Giannini, D. Marinotto, A. Pavanello, A. Previtali, S. Righetto, E. Cariati, Cyclic Triimidazole Derivatives: Intriguing Examples of Multiple Emissions and Ultralong Phosphorescence at Room Temperature, *Angew. Chem. Int. Ed.* 56 (2017) 16302.

[7] E. Lucenti, A. Forni, C. Botta, L. Carlucci, A. Colombo, C. Giannini, D. Marinotto, A. Previtali, S. Righetto, E. Cariati, The Effect of Bromo Substituents on the Multifaceted Emissive and Crystal-Packing Features of Cyclic Triimidazole Derivatives, *ChemPhotoChem* 2 (2018) 801.

[8] E. Lucenti, A. Forni, C. Botta, C. Giannini, D. Malpicci, D. Marinotto, A. Previtali, S. Righetto, E. Cariati, Intrinsic and Extrinsic Heavy-Atom Effects on the Multifaceted Emissive Behavior of Cyclic Triimidazole, *Chemistry - A European Journal* 25 (2019) 2452.

[9] Y. Dong, J. W. Y. Lam, A. Qin, J. Sun, J. Liu, Z. Li, J. Sun, H. H. Y. Sung, I. D. Williams, H. S. Kwok, B. Z. Tang, Aggregation-induced and crystallization-enhanced emissions of 1,2-diphenyl-3,4-bis(diphenylmethylene)-1-cyclobutene, *Chem. Commun.* (2007) 3255.

[10] Y. Dong, J. W. Y. Lam, A. Qin, Z. Li, J. Sun, H. H. Y. Sung, I. D. Williams, B. Z. Tang, Switching the light emission of (4-biphenylyl)phenyldibenzofulvene by morphological modulation: crystallization-induced emission enhancement, *Chem. Commun.* (2007) 40.

[11] D. M. Schubert, D. T. Natan, D. C. Wilson, K. I. Hardcastle, Facile Synthesis and Structures of Cyclic Triimidazole and Its Boric Acid Adduct, *Cryst. Growth Des.* 11 (2011) 843.

[12] E. Lucenti, A. Forni, C. Botta, A. Colombo, C. Giannini, D. Malpicci, D. Marinotto, A. Previtali, S. Righetto, E. Cariati, *Submitted*

[13] G. Gritzner, J. Kuta, Recommendations on reporting electrode potentials in nonaqueous solvents, *Pure Appl. Chem.* 56 (1984) 461.

[14] P. J. Elving, S. J. Pace, J. E. O'Reilly, Electrochemical Reduction of Purine, Pyrimidine, and Imidazole in Aqueous Media. Kinetics and Mechanisms, *J. Am. Chem. Soc*. 95 (1973) 647.

[15] H.-L. Wang, R. M. O'Malley, J. E. Fernandez, Electrochemical and Chemical Polymerization of Imidazole and Some of Its Derivatives, *Macromolecules* 27 (1994) 893.

[16] S. Arnaboldi, R. Cirilli, A. Forni, A. Gennaro, A. A. Isse, V. Mihali, P. R. Mussini, M. Pierini, S. Rizzo, F. Sannicolò, Electrochemistry and Chirality in Bibenzimidazole Systems, *Electrochimica Acta* 179 (2015) 250.

[17] Y. Takeuchi, K. L. Kirk, L. A. Cohen, Imidazole Cyclotrimers (Trimidazoles), a Novel Heteroannular Series, *J. Org. Chem.* 44 (1979) 4243.

[18] K. Izutsu, Electrochemistry in Nonaqueous Solutions, Second, Revised and Enlarged Edition, Wiley-VCH, Weinheim, 2009.

[19] A. A. Isse, G. Berzi, L. Falciola, M. Rossi, P. R. Mussini, A. Gennaro, Electrocatalysis and electron transfer mechanisms in the reduction of organic halides at Ag, *J. Appl. Electrochem.* 39 (2009) 2217.

[20] D. M. Buck, D. Kunz, Triazine Annelated NHC Featuring Unprecedented Coordination Versatility, *Organometallics* 34 (2015) 5335.

[21] J.-M. Savéant, Elements of Molecular and Biomolecular Electrochemistry, Wiley, New Jersey, 2006 (Chapter 3).

[22] J.-M. Savéant, A simple model for the kinetics of dissociative electron transfer in polar solvents. Application to the homogeneous and heterogeneous reduction of alkyl halides, *J Am Chem Soc* 109 (1987) 6788.

[23] C. P. Andrieux, A. Le Gorande, J.-M. Savéant, Electron transfer and bond breaking. Examples of passage from a sequential to a concerted mechanism in the electrochemical reductive cleavage of arylmethyl halides, *J. Am. Chem. Soc.* 114 (1992) 6892.

[24] C.P. Andrieux, J.-M. Savéant, A. Tallec, R. Tardivel, C. Tardy, Concerted and Stepwise Dissociative Electron Transfers. Oxidability of the Leaving Group and Strength of the Breaking Bond as Mechanism and Reactivity Governing Factors Illustrated by the Electrochemical Reduction of α-Substituted Acetophenones, *J. Am. Chem. Soc.* 119 (1997) 2420.

[25] C. P. Andrieux, J.-M. Savéant, C. Tardy, Transition between Concerted and Stepwise Dissociative Electron Transfers. An Example of How a Change of Temperature May Trigger a Change in Mechanism in Electrochemical Experiments, *J. Am. Chem. Soc.* 119 (1997) 11546.

[26] L. Pause, M. Robert, J.-M. Savéant, Can single-electron transfer break an aromatic carbon−heteroatom bond in one step? A novel example of transition between stepwise and concerted mechanisms in the reduction of aromatic iodides, *J. Am. Chem. Soc.* 121 (1999) 7158.

[27] C. Costentin, M. Robert, J.-M. Savéant, Successive removal of chloride ions from organic polychloride pollutants. Mechanisms of reductive electrochemical elimination in aliphatic gem-polychlorides, α,β-polychloroalkenes, and α,β-polychloroalkanes in mildly protic medium, *J. Am. Chem. Soc.* 125 (2003) 10729.

[28] L. Pause, M. Robert, J.-M. Savéant, Stabilities of ion/radical adducts in the liquid phase as derived from the dependence of electrochemical cleavage reactivities upon solvent, *J. Am. Chem. Soc.* 123 (2001) 11908.

[29] M. Fedurco, C.J. Sartoretti, J. Augustynski, Medium effects on the reductive cleavage of the carbon-halogen bond in methyl and methylene halides, J. Phys. Chem. B 105 (2001) 2003.

[30] S. Arnaboldi, A. Gennaro, A. A. Isse, P. R. Mussini, The solvent effect on the electrocatalytic cleavage of carbon-halogen bonds on Ag and Au, *Electrochimica Acta* 158 (2015) 427.

[31] S. Arnaboldi, A. Bonetti, E. Giussani, P. R. Mussini, T. Benincori, S. Rizzo, A. A. Isse, A. Gennaro, Electrocatalytic reduction of bromothiophenes on gold and silver electrodes: An example of synergy in electrocatalysis, *Electrochem. Commun.* 38 (2014) 100.

[32] A. A. Isse, P. R. Mussini, A. Gennaro, New Insights into Electrocatalysis and Dissociative Electron Transfer Mechanisms: The Case of Aromatic Bromides, *J. Phys. Chem. C* 113 (2009) 14983.

[33] D. A. Khobragade, S. G. Mahamulkar, L. Pospisil, I. Cisarova, L. Rulisek, U. Jahn, Acceptor-Substituted Ferrocenium Salts as Strong, Single-Electron Oxidants: Synthesis, Electrochemistry, Theoretical Investigations, and Initial Synthetic Application, *Chem. Eur. J.* 18 (2012) 1226.

[34] W. F. Sokol, D. H. Evans, K. Niki, T. Yagi, Reversible Voltammetric Response for a Molecule Containing Four Non-Equivalent Redox Sites with Application to Citochromo c_3 of *Desulfo Vibrio Vulgaris*, Strain Miyazaki, *J. Electroanal. Chem.* 108 (1980)107.

[35] C. Moreno, A. Campos, M. Teixeira, J. LeGall, M. I. Montenegro, I. Moura, C. van Dijk, J. G. J. Moura , Simulation of the electrochemical behavior of multi-redox systems, *Eur. J. Biochem.* 202 (1991) 385.

[36] A. J. Bard, L. R. Faulkner, Electrochemical Methods: Fundamentals and Applications, 2nd Edition, John Wiley and Sons, Inc., NJ, 2001.

[37] A. A. Isse, S. Arnaboldi, C. Durante, A. Gennaro, Electrochemical reduction of organic bromides in 1-butyl-3-methylimidazolium tetrafluoroborate, *J. Electroanal. Chem.* 804 (2017) 240.

[38] L. Falciola, A. Gennaro, A. A. Isse, P. R. Mussini, M. Rossi, The solvent effect in the electrocatalytic reduction of organic bromides on silver, *J. Electroanal. Chem.* 593 (2006) 47.

[39] A. Ignaczak, J.A.N.F. Gomes, Quantum calculations on the adsorption of halide ions on the noble metals, *J. Electroanal. Chem.* 420 (1997) 71.

[40] G. Valette, Energies involved in the specific adsorption of halides on sd metals. Part I. Analysis of experimental results, *J. Electroanal. Chem.* 255 (1988) 215.

[41] L. Falciola, P. R. Mussini, S. Trasatti, L. M. Doubova, Specific adsorption of bromide and iodide anions from nonaqueous solutions on controlled-surface polycrystalline silver electrodes, *J. Electroanal. Chem.* 593 (2006) 185.

[42] E. Palecek, New trends in electrochemical analysis of nucleic acids, *Bioelectroch. Bioener.* 20 (1988) 179.

Table 1. Key parameters for the reductive electrocleavage of C–X bond for the model molecule **Br-Im** and for the halo-triazoles in DMF + $TBAPF_6$ 0.1M; from CV patterns.

Sample	GC electrode		Au electrode			Ag electrode		
	E_p [a]	α [b]	E_p [a]	α [b]	$\Delta E_{Au–GC}$ /V [c]	E_p [a]	α [b]	$\Delta E_{Ag–GC}$ /V [c]
Br-Im	–3.26	0.32						
1BrTT	–3.01	0.32	–2.38 [d]	n.a.	0.63	–2.51	0.29	0.50
2BrTT	–3.04	0.29	–2.49	n.a.	0.55	–2.62	0.31	0.42
3BrTT	–3.00	0.27	–2.6 [e]	n.a.	ca. 0.4	–2.59	0.29	0.41
1ITT	–2.55	0.32	–1.61	0.30	0.94	–1.42 [f]; –1.82 [g]	n.a.	1.13; 0.73
2ITT	–2.52	0.29	–1.64	0.29	0.88	–1.49 [f]; –1.84 [g]	n.a.	1.03; 0.68

[a] reduction peak potential in V vs $Fc^+|Fc$, at 0.2 V s^{-1}.
[b] Average of the values derived from $E_p - E_{p/2}$ (eq. 4) and $\partial E_{p,c}/\partial \log \upsilon$ (eq. 5).
[c] $\Delta E_{X–GC} = E_{p,X} – E_{p,GC}$, with X stands for Au or Ag electrode.
[d] At 0.05 V s^{-1}.
[e] Approximate value, due to background discharge
[f] pre-peak with a pseudo-capacitive behaviour
[g] Very sharp peak

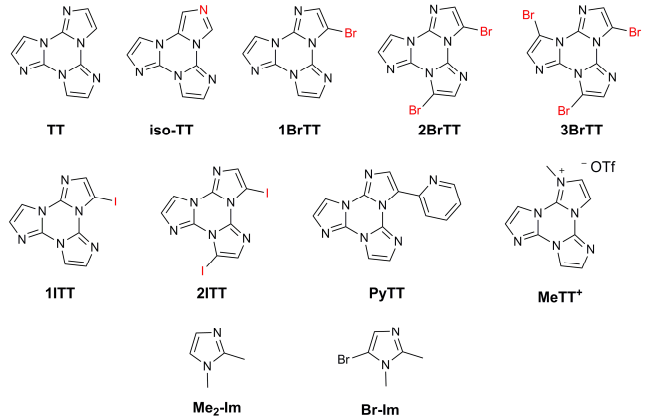

Figure 1. Chemical structures of triimidazotriazines (**TT**s) and related model molecules (**Me_2-Im** and **Br-Im**).

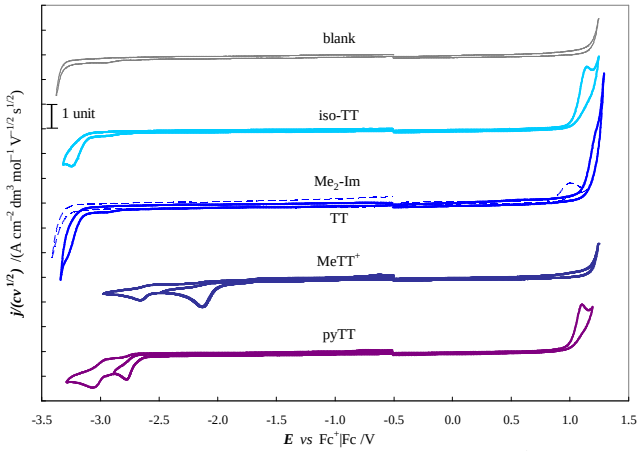

Figure 2. Cyclic voltammetry patterns on GC electrode at 0.2 Vs^{-1} in DMF + $TBAPF_6$ 0.1 M for the non-halogenated **TT** derivatives (solid lines) and the model **Me_2-Im** (dashed line).

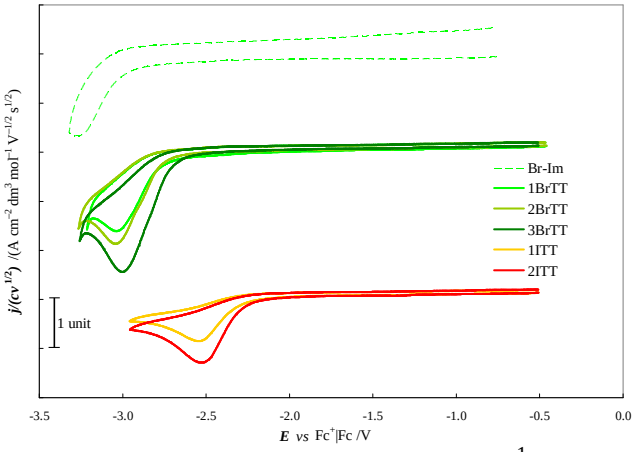

Figure 3. Cyclic voltammetry patterns on GC electrode at 0.2 Vs^{-1} in DMF + $TBAPF_6$ 0.1 M for the halogenated **TT** derivatives (solid lines) and the model **Br-Im** (dashed line). Only the reduction processes are reported.

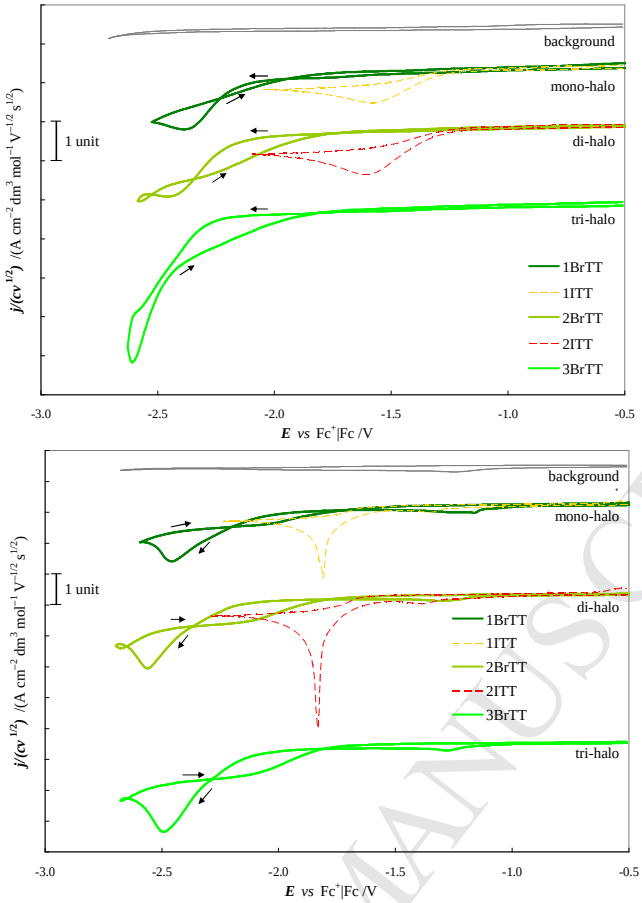

Figure 4. Cyclic voltammetry patterns on Au (top) and Ag (bottom) electrode at 0.05 Vs^{-1} in DMF + $TBAPF_6$ 0.1 M for the **bromoTT** (solid thick lines) and **iodoTT** (dashed thin lines) derivatives. For the bromoTT series arrows indicate directions of the potential scan.

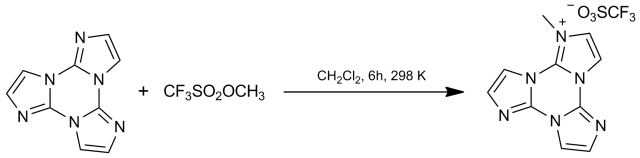

Chart 1. Reaction scheme for **MeTT**$^+$ synthesis.

Highlights:

- Electrochemistry of heteroaromatic compounds widens to cyclic triazines
- Structure/electroactivity study was carried out on a family of triimidazo-triazine
- Weak interaction between equivalent redox sites was detected
- Carbon-halogen bonds break through a dissociative electron transfer (DET)
- Higher electrocatalytic activity was detected for Au electrode with respect to Ag